OIST OKINAWA INSTITUTE OF SCIENCE AND TECHNOLOGY GRADUATE UNIVERSITY
沖縄科学技術大学院大学

Aggregation vs Surface Segregation: Antagonism over the Magnetic Behavior of NiCr Nanoparticles

Author	Murtaza Bohra, Vidya Alman, Arun Showry, Vidyadhar Singh, Rosa E. Diaz, Mukhles Sowwan, Panagiotis Grammatikopoulos
journal or publication title	ACS Omega
volume	5
number	51
page range	32883-32889
year	2020-12-14
Publisher	American Chemical Society
Rights	(C) 2020 American Chemical Society.
Author's flag	publisher
URL	http://id.nii.ac.jp/1394/00001746/

doi: info:doi/10.1021/acsomega.0c03056

ACS AuthorChoice (https://pubs.acs.org/page/policy/authorchoice_termsofuse.html)

This is an open access article published under an ACS AuthorChoice License, which permits copying and redistribution of the article or any adaptations for non-commercial purposes.

ACS OMEGA

http://pubs.acs.org/journal/acsodf

Article

Aggregation vs Surface Segregation: Antagonism over the Magnetic Behavior of NiCr Nanoparticles

Murtaza Bohra,* Vidya Alman, Arun Showry, Vidyadhar Singh, Rosa E. Diaz, Mukhles Sowwan, and Panagiotis Grammatikopoulos*

Cite This: *ACS Omega* 2020, 5, 32883−32889

Read Online

ACCESS | Metrics & More | Article Recommendations | Supporting Information

ABSTRACT: Annealing is a valuable method for fine-tuning the ultrasmall magnetic properties of alloy nanoparticles (NPs) by controlling their sizes, modifying their surfaces, and affecting their magnetic interactions. Herein, we study the effect of moderate annealing (450 °C) on strongly interacting NiCr nanoparticle assemblies (0 ≤ atom % Cr ≤ 15) immediately after deposition. Concurrent temperature-dependent electron microscopy and magnetization data demonstrate the interplay of two competing factors, namely, enhanced particle aggregation and element-specific surface segregation, on the magnetic properties, with the former boosting and the latter suppressing them. Strong interparticle interactions can lead to a magnetic response different from that of superparamagnetic particles, namely, from canonical spin-glass (0 atom % Cr) to correlated spin-glass (5−15 atom % Cr) behavior below higher spin-glass transition temperatures T_g (20−350 K). The observation of "*high-field susceptibility*" below cryogenic temperatures (≤20 K) is ascribed to the presence of inhomogeneity/defects caused by Cr segregation. This work emphasizes the necessity of taking into account the delicate balance of such competing factors to understand the magnetic properties of nanoparticulate samples.

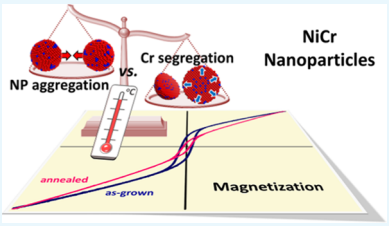

INTRODUCTION

The continuous demand for miniaturization of device components is an important driving force for the magnetic, biomedical, and nuclear industries. In light of this current thrust, MCr (where M = Fe, Co, Ni) alloy nanoparticles (NPs) have been proposed as a potential contender for hard disk drives, drug delivery, and nuclear or water waste management due to their small size, low cost, tunable magnetism, and nanodetection capability.[1−4] However, the controlled synthesis of these NPs encounters various obstacles (such as element-specific surface segregation),[5] whereas their potential use in real-world applications is hindered by their superparamagnetic nature[6] or their limited ability to operate under harsh atmospheres.[7]

Regarding the former issue, we recently investigated the synthesis of NiCr (0−15 atom % Cr) NPs with Curie temperatures that can be tuned near the human body temperature by appropriate Cr doping;[8] such nanoalloys can find direct application in magnetic hyperthermia-based cancer treatment. We found that at 5 atom % Cr, the NPs suffered from substantial Cr-surface segregation, which subsided at 15 atom % Cr, thus drastically affecting their magnetic properties. Various possible ways to control the magnetic properties of MCr NPs have been reported, either by embedding them into noble material matrices,[9] by appropriate doping,[8] or by protecting them within core−shell type structures.[10] An alternative, cost-effective way to obtain desired bulklike magnetic properties in NiCr NPs can be by postgrowth annealing, which is yet to be explored in depth. This is the approach followed in the current work because it enables zooming in on the aforementioned effect of Cr concentration on surface segregation.

Conventional rapid annealing is a typical approach for tailoring the magnetic properties of magnetic alloys such as the stabilization of high-temperature magnetic phases, the induction of magnetic anisotropy, and the enhancement of magnetization/coercivity values.[10−13] Nevertheless, very few studies have been reported on modifying the soft ferromagnetic properties (high saturation magnetization, high remanence ratio, and low coercivity) of interacting NiCr NPs by annealing compared with, e.g., those detailing the growth of the Ni/NiO core−shell structure.[7,14] Sundararajan et al. observed an unexpectedly high saturation magnetization in $Ni_{95}Cr_5$ NPs when subjected to annealing at 600 °C in ambient Ar gas, even higher than that of pure-Ni NPs under the same conditions.[7,10] They attributed this to the presence of Cr, which acts as a catalyst for the rapid growth and aggregation of nanoclusters. However, annealing of $Ni_{95}Cr_5$ NPs at 450 °C under high vacuum of ∼10^{-7} mbar via two different routes has previously given us contradictory results.[5] While ex situ annealing (with the presence of a field of 1 kOe) showed

Received: June 24, 2020
Accepted: October 15, 2020
Published: December 14, 2020

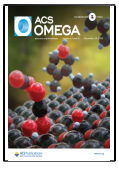

ACS Publications

© 2020 American Chemical Society

https://dx.doi.org/10.1021/acsomega.0c03056
ACS Omega 2020, 5, 32883−32889

complete Cr-surface segregation and magnetic properties typical for pure-Ni NPs (T_C of 635 K), in situ annealing (without a field) yielded low saturation magnetization compared with the as-grown state. Strictly speaking, one cannot directly compare the results of the study by Sundararajan et al. to those of ours because prior to annealing they exposed the NPs to an oxygen atmosphere and the NP sizes were significantly larger (50 nm) than those of ours (5−10 nm). Moreover, an understanding of the effect of particle aggregation and surface segregation on the magnetic properties of dense MCr NP assemblies is still lacking.[7,10,14] This topic is of considerable interest from a fundamental as well as an applied research standpoint, as both miscibility and magnetic properties often vary at the nanoscale with respect to the bulk phase.

A more definitive conclusion could be drawn from annealing in high vacuum; therefore, in the current study it was imperative to investigate the entire magnetic range ($0 \geq$ atom % Cr ≥ 15) of NiCr NPs. Annealing-induced particle aggregation and elemental segregation affected various magnetic properties (magnetization, spin-glass behavior, and high-field susceptibility) in nontrivial ways, which were investigated on the basis of intra- vs interparticle magnetic interactions. We propose that NPs of the 15 atom % Cr sample maintaining a solid-solution structure even after annealing (in contrast to lower-Cr-concentration NPs, where practically full segregation occurs) determine a dopant concentration threshold above which the global experimental observables (i.e., the magnetic data) are largely defined by local NP configurations and intraparticle atomic interactions. For lower Cr concentrations, the magnetic behavior of the samples is mainly governed by the overall Cr content, ensemble sample structure, and interparticle interactions.

Moreover, Ni and Cr are two important constituents of stainless steel and various newly proposed high-entropy alloys (e.g., quaternary NiFeCrCo and quinary NiFeCrCoMn and AlNiFeCrCo);[15−17] thus, the investigation of how Cr segregation affects the resulting magnetic properties is of special interest.

RESULTS AND DISCUSSION

The effect of Cr doping on the magnetization of annealed high-coverage samples of all compositions under study (i.e., 0−15 atom % Cr) was investigated first. Zero-field-cooled (ZFC) and field-cooled (FC) magnetizations measured at a low field of 50 Oe are plotted in Figure 1. The ZFC/FC magnetization values of Cr-doped samples are exaggerated by different multiplying factors to allow for their simultaneous presentation and qualitative comparison. All of the ZFC curves present a clear maximum at T_{peak}, which varies nonmonotonically with Cr doping (see the inset, Figure 1). The magnetization (at a fixed field) and T_{peak} values of all Cr-doped samples are significantly decreased compared with those of pure-Ni NPs. The FC and ZFC curves do not exhibit the usual behavior of superparamagnetic (SPM) systems of noninteracting particles; this includes a strong FC−ZFC irreversibility between the two curves (the extrapolated value of FC magnetization at 0 K should be twice the value at ZFC T_{peak}), and a Curie−Weiss-like ($\sim 1/T$) decay of the magnetization showing a rather linear $\sim T$ dependence in the reversible region. These characteristics are fingerprints of strongly interacting particles, which form a highly frustrated system of coupled spins, termed canonic or correlated spin-glass depending on the strength of coupling.[18−20] Additionally, the FC magnetization of pure-Ni NPs slightly decreases in between 275 and 190 K, whereas for temperatures below 190 K, it shows an almost constant trend akin to canonical spin-glass systems.[18−20] In contrast, in the 5−15 atom % Cr samples, FC magnetizations gradually increase below T_{peak}, compared with pure Ni, indicating correlated spin-glass structures.[18−22]

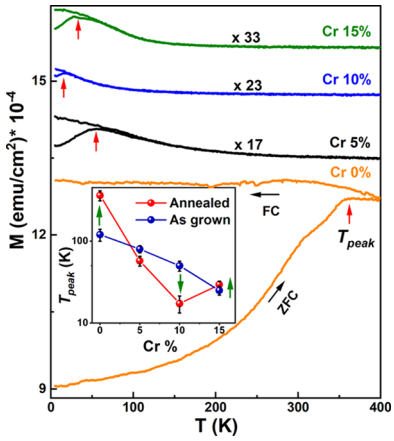

Figure 1. ZFC and FC magnetization curves for annealed NiCr NPs measured at a fixed field (50 Oe). To enable simultaneous observation, M values of Cr-doped samples are exaggerated by different multiplying factors (i.e., by 17, 23, and 33 for 5, 10, and 15 atom % Cr, respectively). Red vertical arrows indicate ZFC maxima, T_{peak}. The inset shows the variation in T_{peak} with Cr atom % doping before and after annealing.

These ZFC/FC magnetic response curves reflect distributions of anisotropy barriers and corresponding switching fields, which are determined by the long-range coupling of spins, more or less independently of the building blocks.[18−20] The switching fields are correlated with the magnetic domain sizes, the anisotropy, and interparticle coupling. The anisotropy depends critically on the shape (classical), the surface (symmetry breaking), and coupling. Furthermore, elemental segregation can significantly alter the anisotropy of the individual constituents. These aspects are discussed in the following paragraphs.

The observed broad peaks of the ZFC curves indirectly indicate the already present non-negligible size distributions (with the corresponding shape variation) for the as-grown samples, as shown in the Supporting Information Figure S2, top row. In pure-Ni and 15 atom % Cr NiCr samples, where Cr-surface segregation due to annealing is either nonexistent (for the former) or very limited (for the latter),[8] Smoluchowski ripening due to annealing (and its ensuing broadening of the size distributions, Figure S3) led to a broadening of the ZFC peaks[23] (Figure S2, bottom row). In the other samples (i.e., 5 and 10 atom % Cr), the ZFC peaks are narrowed down after annealing, indicating the contribution of other, concurrent, effects, which need to be understood.

To compare the chemical ordering between exemplary NPs of the two samples, scanning transmission electron microscopy (STEM) images of annealed 5 and 15 atom % Cr samples (low coverage, for clarity) are demonstrated in Figure 2a,c, respectively. Electron energy loss spectroscopy (EELS) line profiling is shown in Figure 2b and d (for 5 and 15 atom % Cr, respectively), verifying the assumption of suppressed Cr-surface segregation for 15 atom % Cr NPs even after annealing. The presence of Cr-segregates for the 5 atom % Cr sample is

https://dx.doi.org/10.1021/acsomega.0c03056
ACS Omega 2020, 5, 32883−32889

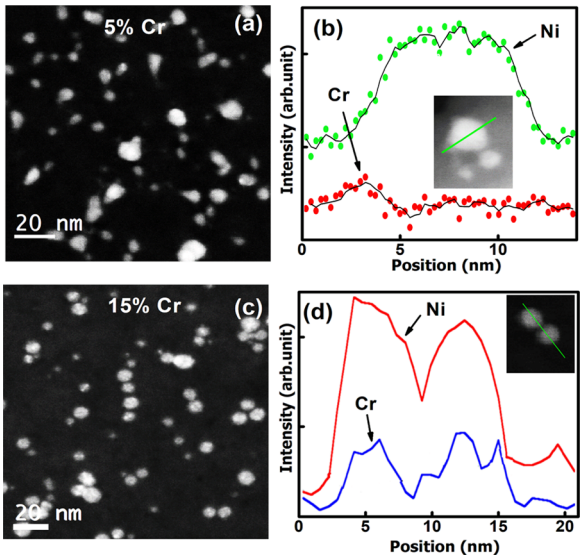

Figure 2. Exemplary STEM images of annealed NiCr alloy NPs of 5 (a) and 15 atom % Cr (c). Corresponding EELS elemental maps in STEM configuration of the indicated NP for Ni $L_{3,2}$ edge and Cr $L_{3,2}$ edge are given in (b) and (d), respectively. EELS Cr line scan from left to right (width: four pixels) of a single NP (inset) 5 atom % Cr (b), suggesting Cr-surface segregation. EELS line scan for two neighboring single NPs 15 atom % Cr (d), indicating that, despite the annealing, a substantial amount of Cr remained at the core of the NPs.

further confirmed by EELS mapping of representative as-grown and annealed NPs in the Supporting Information Figures S4 and S5, respectively.

The aforementioned Smoluchowski ripening and the possibility of enhanced Cr-surface segregation due to the additional thermal energy provided by the annealing constitute two competing factors dictating the magnetic behavior of the annealed samples. It should be noted that the T_{peak} is not identical to blocking temperature (T_B) because of the presence of strong interactions; however, it depends on the size distribution and the field and frequency dependence.[18−22,24] A comparative study of the variation in T_{peak} with Cr doping before and after annealing (see the inset, Figure 1) presents various interesting features:

(i) The T_{peak} of annealed pure-Ni NPs (∼350 K) is almost three times higher than the observed T_{peak} in the as-grown state (∼120 K). This result is expected due to the consolidation of NPs and the growth of their sizes upon annealing. Moreover, the observation of T_{peak} values beyond room temperature is significant and indicative of the strong interparticle interaction.

(ii) For the 5−10 atom % Cr samples, an increase in T_{peak} values would be expected for ordered NiCr NPs after annealing not only due to the increase in NP sizes (just like for the pure-Ni NPs) but also because additional Cr-surface segregation leads to NP cores consisting mainly of Ni.[8] However, the opposite trend is observed, due to the presence of the said Cr-segregates playing a more significant role in decoupling the magnetic interactions among the NPs.[8]

(iii) The T_{peak} of the 15 atom % Cr sample is again increased compared with its as-grown state (as well as compared with that of the 10 atom % Cr sample). This increase can be attributed to the fact that, apparently, the extra thermal energy did not suffice for significant additional Cr segregation due to the high diffusion barriers for Cr precipitates, as explained in ref 8. As a result, remnant Cr was found throughout the NPs (as in the as-grown state) and the annealed $Ni_{85}Cr_{15}$ NPs are merely increased in size, showing magnetic properties which approach those of the bulk $Ni_{85}Cr_{15}$ or are akin to the behavior of pure-Ni NPs.

A comparison of all of the aforementioned features implies that the suppression of *interparticle* interactions due to the presence of Cr-segregates is more important than the atomic scale, *intraparticle* interactions between Ni and Cr atoms. We attribute this behavior to the fact that Cr precipitates, albeit small in size, positioned in between almost pure Ni clusters (after annealing of the 5−10 atom % Cr samples) prevent the latter from consolidating toward larger, fully fused NPs of a significantly larger size. However, it should be pointed out that even though we emphasize the restructuring of individual NPs, in our annealed dense samples a segregated Cr satellite in between two Ni NP cores would not be very different from a small Cr cluster (which happened to nucleate without mixing with Ni) trapped in a similar position. In other words, the global observables (i.e., the magnetic properties) of these two samples are governed by their overall composition, which, as a result of the deposition method, follows the target stoichiometry. This is not true, however, for the 15 atom % sample, where the mixed chemical ordering of individual NiCr NPs is maintained and the overall magnetic behavior is mostly dictated by local atomic interactions. Apparently, cancellation of ferromagnetic interactions among Ni atoms by antiferromagnetic Cr atoms is not as important as the decoupling of ferromagnetic Ni cores by antiferromagnetic Cr satellites/clusters, and the overall sample magnetization increases, following the annealing-induced grain size increase.

We need to point out that these results and their interpretations are relevant for our specific samples grown under specific conditions and displaying corresponding structural features (NP sizes, coverage, attachment to support, etc.). However, our conclusions can be generalized, at least qualitatively, for other samples or systems, and propose a line of inquiry for future studies.

To elucidate spin-glass behavior further, the field dependence of T_{peak} was studied by varying the applied magnetic field between 50 Oe and 10 kOe. The T_{peak} values given in Figure 3 indicate a linear dependence on $H^{2/3}$. The variation in interaction strength is reflected in the different slopes of the linear fittings.[22] Extrapolation of the line to $H = 0$ designates the spin-glass transition temperature (T_g) spanning 20−420 K. When extrapolated toward $T_{peak} = 0$ K, all lines converge to a critical cooling field $H_{crit} \geq 1$ kOe, which indicates that the spin-glass can disappear when $H \geq H_{crit}$. Moreover, merely having a linear relation between T_{peak} and $H^{2/3}$ does not enable distinguishing between SPM and spin-glass states in the presence of strong interactions between NPs. According to Dormann et al.,[25] $H^{2/3}$ vs reduced temperature (T_{red}) scaling should shift with respect to the origin in the non- or weak-interacting NPs. The inset of Figure 3 shows $H^{2/3}$ vs T_{red} lines, where the reduced temperature is defined as $T_{red} = 1 - [T_{peak}(H)/T_g]$. No shift of the line with respect to the origin is observed in pure-Ni and 15 atom % Cr samples, indicating canonical spin-glass behavior as expected for a system with strong interactions. However, a slight shift is observed for the 10 atom % Cr sample, which has relatively weak interactions

https://dx.doi.org/10.1021/acsomega.0c03056
ACS Omega 2020, 5, 32883−32889

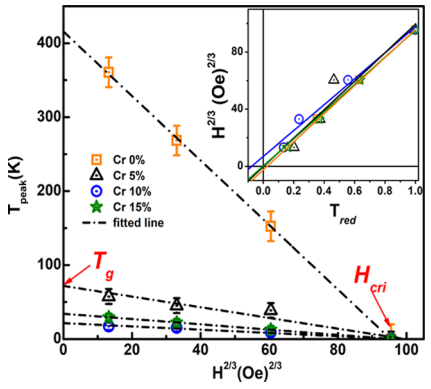

Figure 3. Field dependence of T_{peak} for all NiCr NPs (0−15 atom % Cr) demonstrates a high spin-glass transition temperature, T_g, obtained by extrapolating the line to $H = 0$. The inset shows line plots of $H^{2/3}$ vs reduced temperature, $T_{red} = 1 - [T_{peak}(H)/T_g]$, confirming spin-glass behavior.

and the lowest T_{peak} value and shows features of correlated spin-glass behavior.[22] After annealing, the presence of dipolar interactions among randomly distributed ferromagnetic and antiferromagnetic regions, coupled with additional magnetic frustration caused by Cr-segregates, may lead to a collective spin-glass state with a relatively high T_g.[21]

Having recognized spin-glass-like behavior in annealed NiCr NPs, in what follows, we examine how various anisotropies may affect the shape of low-temperature $M-H$ loops. To investigate this aspect in detail, normalized $M-H$ loops (5 K) are plotted in Figure 4a, juxtaposed with their respective as-

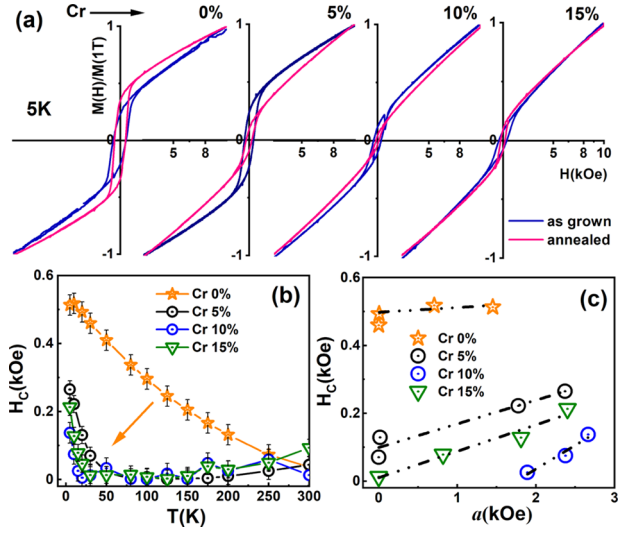

Figure 4. (a) $M(H)/M(1T)$ vs field curves (taken at 5 K) for as-grown and annealed NiCr NPs. (b) H_C vs T curves in between 5 and 300 K for annealed NiCr NPs. (c) An almost linear correlation is found between H_C and a at a low-temperature interval, 5−20 K, for annealed NiCr NPs.

grown state data. There exists a marked nonsaturation effect in the annealed Cr-doped samples, even at the highest magnetic fields of 10 kOe. Generally speaking, the nonsaturation at high field, also called "high-field susceptibility" (HFS), should be significantly lower after annealing.[26] However, the HFS increases after annealing in Cr-doped samples, while in the pure-Ni sample it follows the expected trend. Typically, the contributions to the variation in magnetization under a high field can be attributed to magnetic anisotropy, spin-wave excitation, inhomogeneous spin structures, and lattice defects. This unusually high HFS can be better understood by using the law of approach to saturation[26−29]

$$M = M_S\left(1 - \frac{a}{\sqrt{H}} - \frac{b}{H^2}\right) \quad (1)$$

where M_S is saturation magnetization and a and b are constant coefficients. The $a/\sqrt{H}$ and b/H^2 terms are attributed to the pointlike defects (or magnetic anisotropy fluctuations at the atomic scale) and the weak and large-scale fluctuations in bulk anisotropy, respectively. A reasonable $M-H$ loop fitting can be obtained by the $1/\sqrt{H}$ term with positive a coefficient in a high-field range 5 kOe < H < 10 kOe. Since the coefficient b is related to the bulk magnetic anisotropy constant, K_V, by the relation[27] $b = \frac{4K_V^2}{15M_S^2}$ (and if we leave defects (a) out of consideration), then HFS has to first occur right below T_g because strong interactions can lead to a spin-glass state with high anisotropy. However, observation of high HFS at very low temperatures (5−20 K) indicates that factors other than K_V have to be responsible. The estimated values of the a coefficient for the annealed NiCr NPs, shown in Table 1,

Table 1. Variation of H_C and a Coefficient in Annealed and As-Grown NiCr NPs at 5 K

sample	annealed		as-grown	
Cr (atom %)	H_C (Oe)	a (Oe)	H_C (Oe)	a (Oe)
0	510	1445	600	1995
5	265	2370	430	1700
10	137	2665	395	2385
15	210	2400	365	2360

increase not only with increasing Cr concentration (that is, it reaches a maximum at 10 atom % Cr for the same reasons explained previously) but also from their values for respective as-grown samples. The $1/\sqrt{H}$ approach to saturation further ascertains correlated spin-glass behavior in Cr-segregated NiCr NPs (as shown in Figure 1), which is normally observed in structurally disordered soft magnetic alloys with weak random anisotropy.[30,31]

Furthermore, the coercivity value (H_C) drops in Cr-doped samples, as shown in the low-field range (0−1 kOe) of the $M-H$ loops (Figure 4a). Nevertheless, a rapid increase in H_C values can be observed in NiCr NPs compared with pure-Ni NPs below their T_{peak} temperatures (indicated by the orange arrow in Figure 4b), as expected in spin-glass systems. The H_C typically depends on several factors such as magnetic anisotropy, defects, strain, size, doping, nature of the surface, interface, as well as interparticle interaction. A reasonably good correlation between H_C and a values in Figure 4c implies that both are affected in a similar fashion by the same factors. Thus, nanodefects associated with Cr-segregates not only reduce magnetic interaction among NiCr NPs but also contribute to surface spin canting that may be responsible for HFS. Since in the present case HFS mainly depends on the a coefficient and not fully on K_V, the higher values of a are ascribed to the setting of some sort of surface anisotropy at very low temperatures, which may control both HFS and H_C values. The total anisotropy can be given as the sum of three

https://dx.doi.org/10.1021/acsomega.0c03056
ACS Omega 2020, 5, 32883−32889

contributions, volume (K_V), surface (K_S), and shape (K_{sh}) anisotropies, assuming that NiCr NPs are no longer spherical after annealing, $K_{sh} \neq 0$

$$K_T = K_V + \frac{6}{D}K_S + K_{sh} \quad (2)$$

where S is the surface area.[32−34] Normally, at low temperatures, short-range interactions due to surface spin rearrangement can eventually dominate the collective behavior of the particles.[32] In the present case, apart from bulk macroscopic properties being affected by Cr-surface segregation (e.g., enhancement in Curie temperature values),[5] low-temperature magnetic characteristics are also significantly affected in a different fashion, and a new type of surface anisotropy was developed in doped NiCr NPs.

CONCLUSIONS

We synthesized assemblies of interacting bimetallic NiCr NPs using a cluster beam deposition method and studied their magnetic properties after high-vacuum annealing. In particular, we investigated how annealing-enhanced particle aggregation and element-specific surface segregation compete with each other, yielding contrasting magnetic properties. (i) Up to 10 atom % Cr doping, Cr-surface segregation dominates (although NP aggregation does occur), with Cr-segregates acting as barriers and weakening interparticle magnetic coupling among the ferromagnetic Ni components of the NPs; this results in lower magnetization, T_{peak}, and H_C values. In contrast, at 15 atom % Cr doping, the aggregation effect is dominant; Cr atomic diffusion is more energetically costly (since small sessile Cr precipitates from inside the NPs) and, as a result, non-negligible amounts of Cr remain throughout the NPs. At the same time, growth in NP sizes modifies the overall magnetic characteristics, rendering them similar to those of magnetically ordered Ni NPs. (ii) The observed linear relation between T_{red} and $H^{2/3}$ in strongly magnetically coupled NiCr NPs confirms magnetic behavior akin to a spin-glass state. (iii) Finally, defects like Cr-segregates induce surface anisotropy at very low temperatures, which causes large HFS effects. Furthermore, we established that the global observables (magnetic data) can be, under specific conditions, strongly sensitive to the local properties (chemical ordering); in the current study, this condition refers to Cr concentration. This approach can be generalized for future studies of other M-antiferromagnetic (where M can be Cr, α−Mn, etc.) and M-paramagnetic (where M can be Cu, Al, Ti, etc.) alloy NPs.

EXPERIMENTAL METHODS

$Ni_{100-x}Cr_x$ ($0 \leq x \leq 15$) NPs were synthesized by magnetron sputtering inert-gas condensation (Nanogen50 Source, Mantis Deposition Ltd., U.K.)[35] at a sputtering power of 40 W from nominal compositional alloy targets, as described elsewhere.[8] After substrate landing, NP-loaded Si(100) substrates were load-lock transferred to an inert-gas (N_2) glovebox (maintained at oxygen <0.1 ppm and moisture <1.2 ppm) and characterized by atomic force microscopy (AFM) to determine their coverage (Supporting Information, Figure S1). Subsequently, high-coverage samples were in situ annealed at 450 °C under a vacuum of 1.0×10^{-7} mbar. To prevent surface oxidation for the study of the magnetic properties, these NPs were fully capped by a G-varnish (GE7031) epoxy capping (60−80 nm) inside the glovebox immediately after the annealing.[36] Magnetic properties were measured using a Quantum Design physical property measurement system (PPMS). The diamagnetic contribution from Si substrates was subtracted from the $M-H$ and $M-T$ data by measuring the magnetic susceptibility of the bare Si substrate of known mass. Magnetization values were normalized by the Si-substrate area (0.35 cm × 0.5 cm) considering similar thicknesses for all samples since all depositions were carried out for the same time period of 1 h. For zero-field-cooled (ZFC) magnetization, the sample was initially cooled to 5 K at a zero field, and then magnetization was measured in the presence of a fixed field upon heating. Subsequently, the field-cooled (FC) magnetization was recorded during cooling in the same field. Ultrathin carbon film and silicon nitride (Si_3N_4) membrane transmission electron microscopy (TEM) grids were used as substrates for TEM and scanning TEM (STEM) analysis of lower-coverage samples, using a Cs-corrected environmental TEM (FEI Titan G2 80−300 kV) operating at 300 kV. The in situ heating studies were performed in STEM mode, using a single-tilt heating holder (Gatan). Moreover, energy-dispersive X-ray (EDX) analysis confirmed the average composition of the nanoalloy, and electron energy loss spectroscopy (EELS) elemental mapping elucidated the structural changes of the nanoalloy after the annealing experiments.

ASSOCIATED CONTENT

Supporting Information

The Supporting Information is available free of charge at https://pubs.acs.org/doi/10.1021/acsomega.0c03056.

STEM images, size distributions, and EELS elemental maps (PDF)

AUTHOR INFORMATION

Corresponding Authors

Murtaza Bohra − *Nanoparticles by Design Unit, Okinawa Institute of Science and Technology Graduate University, Okinawa 904-0495, Japan; Mahindra University École Centrale School of Engineering (MEC), Hyderabad 500043, Telangana, India*; Phone: +917093802884; Email: murtaza.bohra@mahindrauniversity.edu.in

Panagiotis Grammatikopoulos − *Nanoparticles by Design Unit, Okinawa Institute of Science and Technology Graduate University, Okinawa 904-0495, Japan*; orcid.org/0000-0002-0057-6339; Phone: +818064974974; Email: pgrammatikopoulos@oist.jp

Authors

Vidya Alman − *Mahindra University École Centrale School of Engineering (MEC), Hyderabad 500043, Telangana, India*

Arun Showry − *Mahindra University École Centrale School of Engineering (MEC), Hyderabad 500043, Telangana, India*

Vidyadhar Singh − *Nanoparticles by Design Unit, Okinawa Institute of Science and Technology Graduate University, Okinawa 904-0495, Japan; Department of Physics, Jai Prakash University, Chapra 841301, Bihar, India*; orcid.org/0000-0001-8164-4534

Rosa E. Diaz − *Nanoparticles by Design Unit, Okinawa Institute of Science and Technology Graduate University, Okinawa 904-0495, Japan*

Mukhles Sowwan − *Nanoparticles by Design Unit, Okinawa Institute of Science and Technology Graduate University,*

https://dx.doi.org/10.1021/acsomega.0c03056
ACS Omega 2020, 5, 32883−32889

Okinawa 904-0495, Japan; orcid.org/0000-0002-0211-2124

Complete contact information is available at: https://pubs.acs.org/10.1021/acsomega.0c03056

Notes

The authors declare no competing financial interest.

■ ACKNOWLEDGMENTS

Work performed at OIST was supported by funding from the Okinawa Institute of Science and Technology Graduate University (OIST). The authors would like to gratefully acknowledge Stephan Steinhauer for constructive suggestions and help with the analysis of results.

■ REFERENCES

(1) Zhao, J.; Baibuz, E.; Vernieres, J.; Grammatikopoulos, P.; Jansson, V.; Nagel, M.; Steinhauer, S.; Sowwan, M.; Kuronen, A.; Nordlund, K.; Djurabekova, F. Formation Mechanism of Fe Nanocubes by Magnetron Sputtering Inert Gas Condensation. *ACS Nano* **2016**, *10*, 4684.

(2) Kaur, M.; Dai, Q.; Bowden, M.; Engelhard, M. H.; Wu, Y.; Tang, J.; Qiang, Y. Watermelon-Like Iron Nanoparticles: Cr Doping Effect on Magnetism and Magnetization Interaction Reversal. *Nanoscale* **2013**, *5*, 7872.

(3) Hu, J.; Chen, G.; Lo, I. M. C. Selective Removal of Heavy Metals from Industrial Wastewater Using Maghemite Nanoparticle: Performance and Mechanisms. *J. Environ. Eng.* **2006**, *132*, 709.

(4) Khanal, L. R.; Williams, T.; Qiang, Y. High-Temperature Investigation on Morphology, Phase and Size of Iron/Iron-Oxide Core-Shell Nanoclusters for Radiation Nanodetector. *J. Phys. D: Appl. Phys.* **2018**, *51*, No. 255302.

(5) Bohra, M.; Grammatikopoulos, P.; Diaz, R. E.; Singh, V.; Zhao, J.; Bobo, J.-F.; Kuronen, A.; Djurabekova, F.; Nordlund, K.; Sowwan, M. Surface Segregation in Chromium-Doped NiCr Alloy Nanoparticles and its Effect on Their Magnetic Behavior. *Chem. Mater.* **2015**, *27*, 3216.

(6) Kiran Kumar, N. A. P.; Li, C.; Leonard, K. J.; Bei, H.; Zinkle, S. J. Microstructural Stability and Mechanical Behavior of FeNiMnCr High Entropy Alloy under Ion Irradiation. *Acta Mater* **2016**, *113*, 230.

(7) Sundararajan, J. A.; Schimel, T.; Kaur, M.; Qiang, Y.; Wang, C.; Baer, D. R.; Bruemmer, S. M. Heat Treatment on Ni and Cr-Doped Ni Core-Shell Nanoparticle Granular Films. *IEEE Int. Conf. Nanotechnol.* **2011**, 657−667.

(8) Bohra, M.; Grammatikopoulos, P.; Singh, V.; Zhao, J.; Toulkeridou, E.; Steinhauer, S.; Kioseoglou, J.; Bobo, J.-F.; Nordlund, K.; Djurabekova, F.; Sowwan, M. Tuning the Onset of Ferromagnetism in Heterogeneous Bimetallic Nanoparticles by Gas Phase Doping. *Phys. Rev. Mater.* **2017**, *1*, No. 066001.

(9) Bohra, M.; Singh, V.; Grammatikopoulos, P.; Toulkeridou, E.; Diaz, R. E.; Bobo, J.-F.; Sowwan, M. Control of Surface Segregation in Bimetallic NiCr Nanoalloys Immersed in Ag Matrix. *Sci. Rep.* **2016**, *6*, No. 19153.

(10) Sundararajan, J. A.; Kaur, M.; Burns, J.; Wu, Y. Q.; Schimel, T.; Qiang, Y. Cr Doping and Heat Treatment Effect on Core-Shell Ni Nanocluster Film. *J. Mater. Sci.* **2016**, *51*, 10873.

(11) Crisan, A. D.; Vasiliu, F.; Mercioniu, I.; Bartha, C.; Enculescu, M.; Crisan, O. Annealing-Induced High Ordering and Coercivity in Novel L10 CoPt-Based Nanocomposite Magnets. *Metals* **2018**, *8*, No. 466.

(12) Johnson, F.; Garmestani, H.; Chu, S. Y.; McHenry, M. E.; Laughlin, D. E. Induced Anisotropy in FeCo-Based Nanocrystalline Ferromagnetic Alloys (HITPERM) by Very High Field Annealing. *IEEE Trans. Magn.* **2004**, *40*, 2697.

(13) Huajun, Z.; Jinhuan, Z.; Zhenghai, G.; Wei, W. Preparation and Magnetic Properties of Ni Nanorod Arrays. *J. Magn. Magn. Mater.* **2008**, *320*, 565.

(14) Wang, C.-M.; Baer, D. R.; Bruemmer, S. M.; Engelhard, M. H.; Bowden, M. E.; Sundararajan, J. A.; Qiang, Y. Microstructure of the Native Oxide Layer on Ni and Cr-Doped Ni Nanoparticles. *J. Nanosci. Nanotechnol.* **2011**, *11*, 8488.

(15) Ikeda, Y.; Grabowski, B.; Körmann, F. AbInitioPhase Stabilities and Mechanical Properties of Multicomponent Alloys: A Comprehensive Review for High Entropy Alloys and Compositionally Complex Alloys. *Mater. Charact.* **2019**, *147*, 464.

(16) Ming, K.; Li, L.; Li, Z.; Bi, X.; Wang, J. Grain Boundary Decohesion by Nanoclustering Ni and Cr Separately in CrMnFeCoNi High-Entropy Alloys. *Sci. Adv.* **2019**, *5*, No. eaay0639.

(17) Borkar, T.; Chaudhary, V.; Gwalani, B.; Choudhuri, D.; Mikler, C. V.; Soni, V.; Alam, T. V.; Ramanujan, R.; Banerjee, R. A combinatorial approach for assessing the magnetic properties of high entropy alloys: Role of Cr in $AlCo_xCr_{1-x}FeNi$. *Adv. Eng. Mater.* **2017**, *19*, No. 1700048.

(18) Du, J.; Zhang, B.; Zheng, R. K.; Zhang, X. X. Memory effect and spin-glass-like behavior in Co-Ag granular films. *Phys. Rev. B* **2007**, *75*, No. 014415.

(19) Yamamoto, Y.; Hidekazu Tanaka, H.; Kawai, T. The Control of Cluster-Glass Transition Temperature in Spinel-Type $ZnFe_2O_{4-\delta}$Thin Film. *Jpn. J. Appl. Phys.* **2001**, *40*, L545−L547.

(20) De Toro, J. A.; Lee, S. S.; Salazar, D.; Cheong, J. L.; Normile, P. S.; Muñiz, P.; Riveiro, J. M.; Hillenkamp, M.; Tournus, F.; Tamion, A.; Nordblad, P. A nanoparticle replica of the spin-glass state. *Appl. Phys. Lett.* **2013**, *102*, No. 183104.

(21) Nordblad, P. Competing interaction in magnets: the root of ordered disorder or only frustration? *Phys. Scr.* **2013**, *88*, No. 058301.

(22) Peddis, D.; Cannas, C.; Musinu, A.; Piccaluga, G. Coexistence of Superparmagnetism and Spin-Glass Like Magnetic Ordering Phenomena in a $CoFe_2O_4$-SiO_2 Nanocomposite. *J. Phys. Chem. C* **2008**, *112*, 5141.

(23) Stoldt, C. R.; Jenks, C. J.; Thiel, P. A.; Cadilhe, A.M.; Evans, J.W. Smoluchowski Ripening of Ag Islands on Ag(100). *J. Chem. Phys.* **1999**, *111*, 5157.

(24) Tuboltsev, V.; Savin, A.; Sakamoto, W.; Hieno, A.; Yogo, T.; Räisänen, J. Spin-glass behavior of nanocrystalline multiferroic bismuth ferrite leadtitanate. *J. Mater. Chem.* **2011**, *21*, 781.

(25) Dormann, J. L.; Fiorani, D.; El Yamani, M. Field dependence of the blocking temperature in the superparamagnetic model: $H^{2/3}$ coincidence. *Phys. Lett. A* **1987**, *120*, 95.

(26) Dash, J.; Prasad, S.; Venkataramani, N.; Krishnan, R.; Kishan, P.; et al. Study of Magnetization and Crystallization in Sputter Deposited LiZn Ferrite Thin Films. *J. Appl. Phys.* **1999**, *86*, 3303.

(27) Kumar, P. A.; Mitra, S.; Mandal, K. Structural and Magnetic Properties of Co Nanoparticles in Cu/SiO_2 Matrix. *Indian J. Pure Appl. Phys.* **2007**, *45*, 21.

(28) Jin, Z.-Q.; Tang, W.; Zhang, J.-R.; Qin, H.-X.; Du, Y.-W. Effective Magnetic Anisotropy of Nanocrystalline Nd-Fe-Ti-N Hard Magnetic Alloys. *Eur. Phys. J. B* **1998**, *3*, 41.

(29) Bohra, M.; Prasad, S.; Venketaramani, N.; Kumar, N.; Sahoo, S. C.; Krishnan, R. Magnetic properties of magnetite thin films close to the Verwey transition. *J. Magn. Magn. Mater.* **2009**, *321*, 3738.

(30) Tejada, J.; Martinez, B.; Labarta, A.; Chudnovsky, E. M. Correlated spin glass generated by structural disorder in the amorphous $Dy_6Fe_{74}B_{20}$ alloy. *Phys. Rev. B* **1991**, *44*, 7698.

(31) Chudnovsky, E.; Serota, R. Correlated spin glass: A new way to extremely soft magnetic materials. *IEEE Trans. Magn.* **1984**, *20*, 1400.

(32) Ridier, K.; Gillon, B.; Chaboussant, G.; Catala, L.; Mazérat, S.; Rivière, E.; Mallah, T. Individual-collective crossover driven by particle size in dense assemblies of superparamagnetic nanoparticles. *Eur. Phys. J. B* **2017**, *90*, No. 77.

(33) Moura, K. O.; Limba, R. J. S.; Coelho, A. A.; Souza-Junior, E. A.; Duque, J. G. S.; Meneses, C. T. Tuning the Surface Anisotropy in Fe-doped NiO Nanoparticles. *Nanoscale* **2014**, *6*, 352.

(34) Singh, V.; Srinivas, V.; Ranot, M.; Angappane, S.; Park, J.-G. Effect of polymer coating on the magnetic properties of oxygen-stabilized nickel nanoparticles. *Phys. Rev. B* **2010**, *82*, No. 054417.

(35) Grammatikopoulos, P.; Steinhauer, S.; Vernieres, J.; Singh, V.; Sowwan, M. Nanoparticle Design by Gas-Phase Synthesis. *Adv. Phys.: X.* **2016**, *1*, 81−100.
(36) Bohra, M.; Singh, V.; Sowwan, M.; Bobo, J.-F.; Chung, C.-J.; Clemens, B. J. Influence of Packaging on the Surface Oxidation and Magnetic Properties of Cobalt Nanocrystals. *J. Phys. D: Appl. Phys.* **2014**, *47*, No. 305002.

https://dx.doi.org/10.1021/acsomega.0c03056
ACS Omega 2020, 5, 32883−32889